

## PUBLISHED VERSION

M. Khalid, G.Y. Chen, J. Bei, H. Ebendorff-Heidepriem and D.G. Lancaster  
**Microchip and ultra-fast laser inscribed waveguide lasers in Yb<sup>3+</sup> germanate glass**  
Optical Materials Express, 2019; 9(8):3557-3564

DOI: <http://dx.doi.org/10.1364/OME.9.003557>

© 2019 Optical Society of America under the terms of the OSA Open Access Publishing Agreement. Users may use, reuse, and build upon the article, or use the article for text or data mining, so long as such uses are for non-commercial purposes and appropriate attribution is maintained. All other rights are reserved.

### PERMISSIONS

[https://www.osapublishing.org/submit/review/copyright\\_permissions.cfm#posting](https://www.osapublishing.org/submit/review/copyright_permissions.cfm#posting)

#### Author and End-User Reuse Policy

OSA's policies afford authors, their employers, and third parties the right to reuse the author's Accepted Manuscript (AM) or the final publisher Version of Record (VoR) of the article as outlined below:

Reuse purpose	Article version that can be used under:		
	Copyright Transfer	Open Access Publishing Agreement	CC BY License
Posting by authors on an open institutional repository or funder repository	AM after 12 month embargo	VoR	VoR

#### Attribution

##### Open access articles

If an author or third party chooses to post an open access article published under OSA's OAPA on his or her own website, in a repository, on the arXiv site, or anywhere else, the following message should be displayed at some prominent place near the article and include a working hyperlink to the online abstract in the OSA Journal:

© XXXX [year] Optical Society of America]. Users may use, reuse, and build upon the article, or use the article for text or data mining, so long as such uses are for non-commercial purposes and appropriate attribution is maintained. All other rights are reserved.




When adapting or otherwise creating a derivative version of an article published under OSAs OAPA, users must maintain attribution to the author(s) and the published article's title, journal citation, and DOI. Users should also indicate if changes were made and avoid any implication that the author or OSA endorses the use.

**29 June 2021**

<http://hdl.handle.net/2440/120914>



# Microchip and ultra-fast laser inscribed waveguide lasers in Yb<sup>3+</sup> germanate glass

M. KHALID,<sup>1,\*</sup> G. Y. CHEN,<sup>1</sup>  J. BEI,<sup>2</sup> H. EBENDORFF-HEIDEPRIEM,<sup>2</sup>  AND D. G. LANCASTER<sup>1</sup> 

<sup>1</sup>Laser Physics and Photonics Devices Laboratories — School of Engineering, University of South Australia, Mawson Lakes, SA 5095, Australia

<sup>2</sup>Institute for Photonics and Advanced Sensing and School of Physical Sciences, University of Adelaide, SA 5005, Australia

\*[khamy062@mymail.unisa.edu.au](mailto:khamy062@mymail.unisa.edu.au)

**Abstract:** We report the first Yb<sup>3+</sup>-doped germanate waveguide laser fabricated using femtosecond direct writing. Positive refractive-index channels were inscribed in Yb<sup>3+</sup> doped high refractive-index (1.85) GPGN glass with molar composition 54.5GeO<sub>2</sub>-31PbO-4Ga<sub>2</sub>O<sub>3</sub>-9Na<sub>2</sub>O-1.5Yb<sub>2</sub>O<sub>3</sub>, resulting in 13 mm long waveguides with a refractive-index change of  $\sim 9 \times 10^{-4}$ . The laser performance is investigated in the unguided microchip and in the waveguide configuration. A maximum output power of  $\sim 51$  mW at 1.052  $\mu\text{m}$  with a slope efficiency of  $\sim 30\%$  and a lasing threshold of 100 mW was achieved from the Yb<sup>3+</sup>: GPGN microchip laser with a 4.5 mm gain length. A maximum output of  $\sim 15$  mW at 1.069  $\mu\text{m}$  with a low lasing-threshold of 83 mW was achieved from the un-optimized 24  $\mu\text{m}$  core-diameter, 13 mm long Yb<sup>3+</sup>: GPGN waveguide laser.

© 2019 Optical Society of America under the terms of the [OSA Open Access Publishing Agreement](#)

## 1. Introduction

In recent years heavy metal oxide glasses like germanate and tellurite have been a research focus as active gain media for laser applications due to advantages over fluorides and silicates [1–4]. Germanate glasses offer advantage over tellurite glasses [3,4] as they share a number of properties with widely used commercial silicate glasses such as high fracture toughness, positive thermo-optic coefficient, high chemical, mechanical and thermal stabilities, and high glass transition temperature. However, unlike silicates, germanates have higher linear and nonlinear refractive indices, lower phonon-energy, and provide a wider transmission window covering  $\sim 0.5$  to 4  $\mu\text{m}$  in a  $\sim 1$  m long fiber [4]. This makes them a good candidate not only for laser applications but also for nonlinear devices such as supercontinuum generation and four-wave mixing [5]. Among the germanate glass family, lead-germanate glass is of particular interest for infrared laser applications as it provides the same low phonon energy and high nonlinearity as widely investigated zinc-tellurite glasses but has  $\sim 100$  °C higher glass transition temperature and therefore considerably higher thermal and mechanical stability compared to zinc-tellurite glasses [3,4]. Na-Ga-lead-germanate glass (GPGN) was shown to have high stability against crystallization, which enabled fabrication of low-loss fiber, making this glass a promising material for infrared laser development [4].

Germanate glasses with various rare earth dopants have been studied spectroscopically for laser applications [6,7]. Ho<sup>3+</sup> and Tm<sup>3+</sup> doped germanate glass fiber lasers have been shown to be reasonably efficient (commensurate with their early stage development) with slope efficiencies of  $\sim 34\%$  [8] and  $\sim 68\%$  [9], respectively. We note that limited work has been done to date on the development of waveguide lasers using germanate glass as the gain medium.

Ultrafast laser inscription (ULI) is an emerging technique for fabricating waveguides, and preferred over other contemporary waveguide fabrication techniques in some cases because of its flexibility in rapidly fabricating new waveguide geometries, and the controllable refractive

index modification in the glass by managing the femtosecond laser parameters [10]. Some studies have reported ultrafast-laser written waveguides in germanate glass where they used 1 kHz, 100 kHz and 500 kHz repetition rates of the femtosecond laser to inscribe waveguides [1,11–13]. Compared to fiber drawing, ULI allows waveguide structures to be produced directly in the as-made glass without further processing steps of preform fabrication and fiber drawing. Therefore, the key attractions of ULI are its ease of implementation, controllable structures, and CNC repeatability to produce chip scale devices [10]. In addition, since passive and active device functionalities can be combined within one integrated chip, our focus is towards ULI made waveguide lasers and amplifiers. To date, to the best of our knowledge, ULI-fabricated waveguide laser and amplifier based on germanate glass have only been reported for 2 wt%  $\text{Tm}_2\text{O}_3$  doped composition  $56\text{GeO}_2 - 31\text{PbF}_2 - 9\text{Na}_2\text{O} - 4\text{Ga}_2\text{O}_3$  with 6% slope efficiency at  $1.9 \mu\text{m}$  [12] and 2 wt%  $\text{Er}_2\text{O}_3$  doped composition  $17\text{GeO}_2 - 73\text{PbO} - 10\text{Ga}_2\text{O}_3$  with internal gain of 2.7 dB/cm at  $1.5 \mu\text{m}$  [13].

In this study, we present the first  $\text{Yb}^{3+}$ -doped germanate microchip laser and waveguide laser. We have selected GPGN lead germanate glass as the host material based on promising results of low-loss fiber fabrication [4] and ULI-fabricated waveguide  $\text{Tm}^{3+}$  laser demonstration [12] for this glass type.  $\text{Yb}^{3+}$  is an efficient laser ion with a simple ion structure, high quantum efficiency, and is routinely used for high power laser applications. In addition,  $\text{Yb}^{3+}$  lasers are pumped with cost-effective 976 nm laser diodes. Therefore,  $\text{Yb}^{3+}$  is an ideal laser ion to investigate new host glasses and is thus utilized in this study for exploring the laser performance of GPGN glass prior to investigating the more challenging problem of achieving longer wavelength transitions. A  $L = 4.5 \text{ mm}$  long  $\text{Yb}^{3+}$ : GPGN chip was utilized in a traditional unguided microchip configuration for the realization of a free-running 1052 nm chip laser with a  $\sim 51 \text{ mW}$  average output power and a  $\sim 30\%$  slope efficiency. To demonstrate the potential of fs-written waveguides in this glass, we also demonstrated laser operation from a guided ( $L = 13 \text{ mm}$ )  $\text{Yb}^{3+}$  doped lead-germanate waveguide laser operating at 1069 nm with a maximum output power of  $\sim 15 \text{ mW}$ , and a low lasing-threshold of  $\sim 83 \text{ mW}$  which demonstrates GPGN to be a promising gain material.

## 2. Glass fabrication and characterization

The lasers were fabricated from a 20 g ingot of 3.6 wt%  $\text{Yb}^{3+}$  doped lead germanate glass with molar composition  $54.5\text{GeO}_2 - 31\text{PbO} - 4\text{Ga}_2\text{O}_3 - 9\text{Na}_2\text{O} - 1.5\text{Yb}_2\text{O}_3$  ( $\text{Yb}^{3+}$ : GPGN) prepared using the widely adopted lead germanate glass melt-quench technique stated in [3,4]. The glass batch was melted in a platinum crucible at  $\sim 1250 \text{ }^\circ\text{C}$  for 2 hours under dry oxygen flow. The molten glass was cast into a preheated brass mould and annealed for 2 hours at  $\sim 400 \text{ }^\circ\text{C}$ . It was post annealed for  $\sim 15$  hours to reduce stress generated within the glass during the casting and cooling in the mould. The cast glass block has dimensions of  $30 \times 15 \times 5 \text{ mm}^3$  and is observed to be optically transparent and homogeneous. The block was divided into two parts, one for developing the microchip laser, and the other used for ULI guiding structures for waveguide laser development. The refractive index of the GPGN glass was measured by an ellipsometer (J.A. Woolam, VB-400 VASE) to be 1.853 at 2000 nm and the density of glass was measured through Archimedes principle to be  $5.61 \pm 0.02 \text{ g/cm}^3$ . Based on the glass density and the  $\text{Yb}^{3+}$  concentration, the  $\text{Yb}^{3+}$  ion density was calculated to be  $7 \times 10^{20} \text{ cm}^{-3}$ .

The absorption spectrum of the  $\text{Yb}^{3+}$ : GPGN glass in the range of 0.3–3  $\mu\text{m}$  was measured using an Agilent Cary 5000 spectrophotometer for determining the ground state absorption for both the pump and the laser wavelengths. The attenuation spectrum in Fig. 1(a) shows the characteristic  $\text{Yb}^{3+}$  absorption band at 976 nm for the  ${}^2\text{F}_{7/2} \rightarrow {}^2\text{F}_{5/2}$  transition. The broad absorption band observed at  $\sim 2.8 \mu\text{m}$  is due to OH group contamination, which is expected to have no effect on the short infrared laser transition of  $\text{Yb}^{3+}$  at  $\sim 1 \mu\text{m}$ . The emission spectrum was measured using a Spectrofluorimeter (Edinburgh Instruments FLS980) and normalized using the Fuchtbauer Ladenburg equation. Figure 1(b) shows the absorption cross section measured

using the Beer-Lambert Law and the emission cross section of the  $\text{Yb}^{3+}$ :GPGN sample. The peak absorption cross section for  $\text{Yb}^{3+}$  in this glass is  $\sim 1.1 \times 10^{-20} \text{ cm}^2$ . The optical gain is calculated to be  $\sim 0.3 \text{ dB}$  for 5 mm path length using the equation  $G = \sigma_e N_2 - \sigma_a N_1$ , where  $\sigma_e$  and  $\sigma_a$  are the effective emission and absorption cross sections of  $\text{Yb}^{3+}$  in the medium and  $N_1$  and  $N_2$  are the number of  $\text{Yb}^{3+}$  ions in the ground state and excited state energy levels.

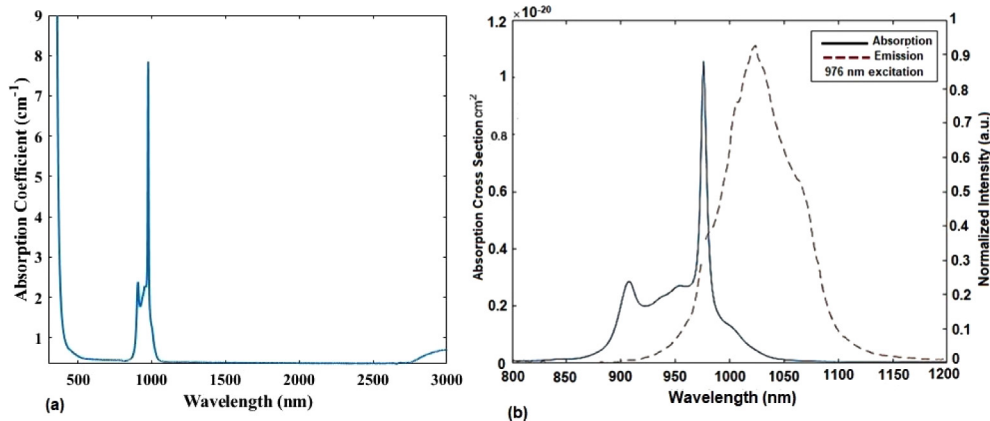


**Fig. 1.** (a) Absorption spectrum of  $\text{Yb}^{3+}$ :GPGN. (b) The measured absorption cross section of the  $\text{Yb}^{3+}$  germanate glass is shown as the solid black line. The normalized emission spectrum of the  $\text{Yb}^{3+}$  germanate glass is shown as the dashed red line.

### 3. Laser development and characterization

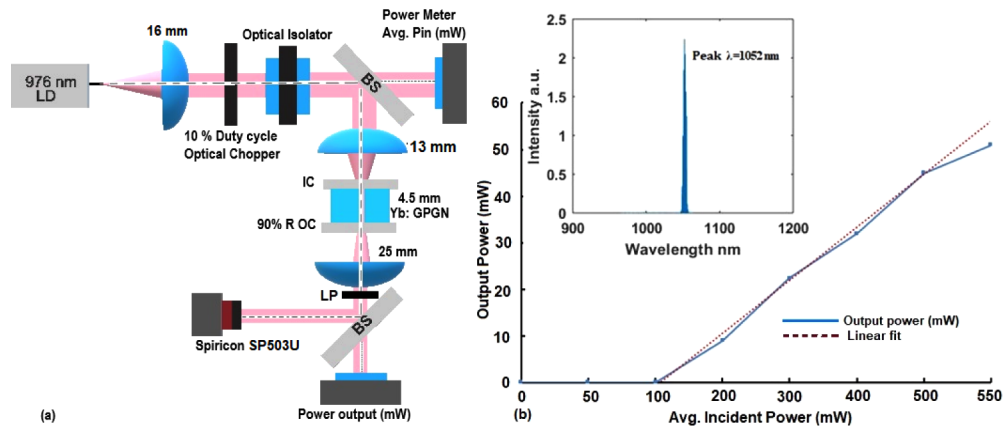
#### 3.1. $\text{Yb}^{3+}$ :GPGN microchip laser

Figure 2(a) shows the experimental setup for the  $\text{Yb}^{3+}$ :GPGN microchip laser. A 976 nm, 10 W, diode laser was delivered via a NA = 0.22, 105  $\mu\text{m}$  multimode fiber. The fiber output was collimated by an anti-reflection (AR) coated  $f = 16 \text{ mm}$  aspheric lens and directed through a 10% duty cycle optical chopper to provide a 10 W peak quasi-continuous wave pump pulse extending for  $\sim 0.11 \text{ ms}$ . The chopper ensured that the average pump power was only  $\sim 1 \text{ W}$ , and the  $\sim 1 \text{ W}$  peak-power laser threshold of the conductively cooled laser assembly could be comfortably achieved. In prior work, thermal fracture of this glass composition occurred at  $\sim 9 \text{ W}$  of average power.

A free-space optical isolator (OI-5-980-VLP) was placed after the optical chopper to attenuate any feedback to the laser diode (to mitigate pump damage). The chopped pump-beam was directed to the laser cavity via a beam sampling mirror which allowed monitoring of the average pump power. For initial work, a  $f = 13 \text{ mm}$  lens was used to focus the 3.5 mm diameter pump beam to  $\sim 60 \mu\text{m}$  diameter ( $1/e^2$ ) with an estimated Rayleigh range of 11.5 mm (using  $z_R = \pi \omega_0^2 / \lambda$ ).

The microchip laser cavity was composed of a  $L = 4.5 \text{ mm}$  thick plane-parallel polished  $\text{Yb}^{3+}$  germanate disk butt-coupled to the input and output-coupler resonator mirrors. The input-coupler (IC) mirror was highly transmitting at 976 nm, and highly reflecting at  $> 1 \mu\text{m}$ . The output-coupler (OC) was 90% reflective for wavelengths between 1 and 1.1  $\mu\text{m}$ . The output beam was collimated using a  $f = 25 \text{ mm}$  lens and passed through long pass (LP) filter to remove the residual pump. A power meter was then used to measure the laser output power.

Figure 2(b) plots the output power from the microchip configured laser showing an incident slope efficiency of  $\sim 30\%$ . The measured wavelength at maximum power was  $\sim 1052 \text{ nm}$  (see inset to Fig. 2(b)). For this length of gain medium (4.5 mm),  $\sim 81\%$  of the pump is absorbed which gives an absorbed slope efficiency of  $\sim 35\%$ . As can be observed from Fig. 2(b), the



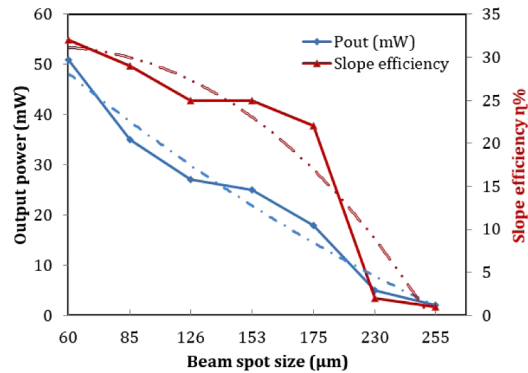
**Fig. 2.** (a) Experimental setup for the  $\text{Yb}^{3+}$ : GPGN microchip laser operating at 1052 nm. A 90% reflective OC and high-transmitting IC is butt-coupled to the chip and laser operation was achieved after 100 mW of average incident pump-power (1 W peak-power) (b) Average output-power obtained by varying the incident  $\lambda = 976$  nm pump-power giving  $\sim 30\%$  incident slope efficiency ( $R = 90\%$  OC). The free-running laser operated with a pump-dependent wavelength between 1050 nm to 1055 nm. A  $\sim 3$  nm FWHM bandwidth emission peaked at 1052 nm is shown in the inset.

output power started to decrease for  $> 500$  mW of pump power, which we attribute to thermal lensing of the gain medium. The thermo-optic coefficient  $dn/dt$  for lead germanate glass is  $\sim 9 \times 10^{-6} \text{ K}^{-1}$ , and its thermal conductivity is  $\kappa \sim 0.7 \text{ W m}^{-1} \text{ K}^{-1}$  [14,15]. Based on these values and using the formula for calculating the focal length,  $f$ , of thermal lensing,  $f^{-1} = \frac{dn/dt}{2\kappa A} P_{in}$ , where  $A$  is the mode area of the waveguide and  $P_{in}$  is the incident power, the focal length of thermal lensing for  $P_{in} = 550$  mW is calculated to be  $\sim 3$  mm, which is shorter than the laser cavity length of 4.5 mm. This confirms that, for  $> 550$  mW input power, thermal lensing affects the overall laser efficiency and also the output beam quality. For lower input power, the focal length of thermal lensing is larger than the laser cavity and thus the laser output power is linear. The efficiency of the laser can be improved using anti-reflection coatings on the glass facets to mitigate the high Fresnel losses in the cavity (9%/facet as  $n \sim 1.86$ ) which will also allow the cavity output-coupling to be optimized.

To optimize the ratio of microchip laser pump-volume to the cavity-mode, the effect of varying the pump-beam size to the efficiency and corresponding output-power of the laser was investigated. By decreasing the pump beam-diameter, the slope efficiency and the output-power of the laser was observed to increase (Fig. 3). Maximum power and slope-efficiency was obtained for a 60  $\mu\text{m}$  spot size. Our reasoning is that the decreasing pump-volume better matches the small cavity mode-diameter and the tighter pump (smaller area) gives a higher population inversion with less ground-state absorption. The pump spot-size could not be focused to less than 60  $\mu\text{m}$  as the shortest focal-length lens that could be configured to couple the pump into the cavity was  $f = 13$  mm.

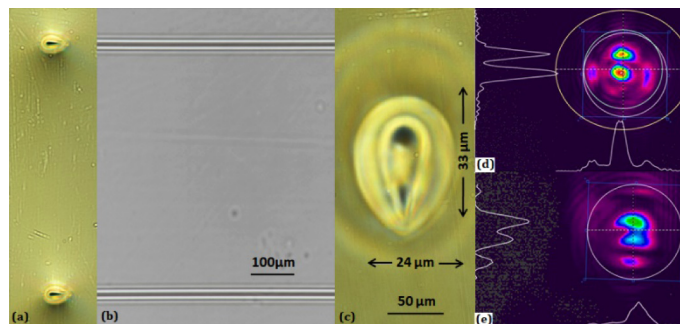
### 3.2. $\text{Yb}^{3+}$ : GPGN waveguide laser

A second laser configuration is reported here based on a 14 mm (length before polishing)  $\text{Yb}^{3+}$ :GPGN chip with 24 bidirectional waveguides. To inscribe the waveguides in our glass sample we concentrated on the ‘thermal regime’ ultra-fast inscription as it is a more rapid waveguide writing technique than the ‘athermal’ regime [16]. The waveguides were written with an ultra-fast laser (IMRA FCPA  $\mu$ -Jewel) frequency doubled to 524 nm and operating at 5



**Fig. 3.** Average output-power vs different spot-sizes (blue diamonds) achieved using different pump-beam focusing conditions. The highest average output-power achieved was  $\sim 51$  mW (peak = 0.51 W) from the smallest beam spot of 60  $\mu\text{m}$ . The red data (triangles) represents the effect of spot-size on the slope efficiency with the highest efficiency obtained from the smallest pump-beam spot.

MHz with pulse durations of 250 fs. To write the waveguides, the glass chip was mounted on an air-bearing x-y-z translation platform (Aerotech ABL9000) and translated at a speed of 1 mm/s. To produce refractive-index modifications, the linearly polarized 250 fs pulses were focused below the surface of the sample using a ZEISS 100X oil-immersion NA = 1.25 microscope objective. The waveguides were written 150  $\mu\text{m}$  below the surface with 300  $\mu\text{m}$  spacing between them. By varying the pulse energies from 15 nJ to 75 nJ waveguide diameters of 12  $\mu\text{m}$  to 80  $\mu\text{m}$  were achieved. Waveguides were found to possess a positive refractive index change. It was observed that no waveguides had any macro or micro-cracks using these parameters. The shape of the written waveguides was elliptical (tear drop) as shown in Fig. 4 due to spherical aberration. The high glass refractive index of 1.85 results in an elongated beam as the objective is designed to focus into a medium with  $n \sim 1.5$ . The shape of the waveguides thus becomes more elliptical as the writing beam focuses deeper into the glass. The end facets of the chip were parallel polished back by  $\sim 500$   $\mu\text{m}$  to reveal the waveguides and produce the final  $L = 13$  mm long waveguides.



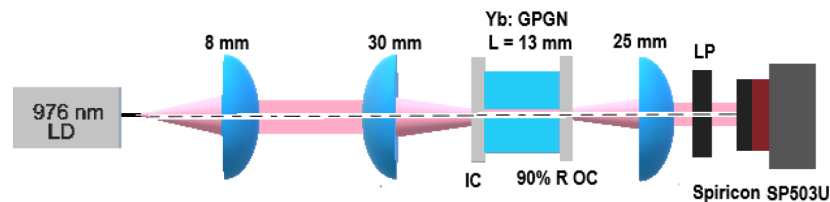
**Fig. 4.** (a)(c) Brightfield microscope image (20X (a) and 50X (c) objective) of 24  $\mu\text{m}$  waveguides written with 5 MHz RR, 20 nJ pulse energy and 1 mm/s translation speed 150  $\mu\text{m}$  underneath the surface producing  $24 \times 33 \mu\text{m}^2$  waveguides. (b) Longitudinal view of the same waveguides showing different layers produced during the ULI writing process. (d) Near field image of pump guidance in laser mode cavity (976 nm pump + 1069 nm laser). (e) Near field image of He-Ne guidance through waveguide for laser cavity mode loss measurements.

Figure 4 shows a brightfield illuminated microscope image of the  $24 \times 33 \mu\text{m}^2$  waveguide that achieved laser operation (pulse energy = 20 nJ, at 1 mm/s). The waveguides displayed a net positive refractive index change in a region greater than the focal volume. Furthermore, the guiding region appeared to have non-uniform refractive index modifications and thus light guidance took place only in the ‘bright’ looking regions surrounding the focal volume as shown in Fig. 4(a) and (c), depicting that the induced waveguides are multimode in nature. Figure 4(d) represents the near-field image of the residual 976 nm pump beam after propagating through the waveguide mode within the laser cavity. Figure 4(e) is the near field image of a red He-Ne laser through the waveguide to measure the optical loss of the laser cavity mode.

The measured propagation loss for the lasing mode of the waveguide in Fig. 4(e) was estimated to be  $< 1.8 \pm 0.1$  dB/cm at 633 nm wavelength taking into account the Fresnel loss but not coupling loss. This loss value is high, partly due to mode mismatch of the symmetrical probe beam and the asymmetric tear-drop structure of the waveguides. Previously reported lead germanate glass waveguides fabricated using the athermal regime had waveguide loss of  $\sim 0.67 \pm 0.33$  dB/cm at 1.9  $\mu\text{m}$  [12]. The similar loss for our waveguides indicates that the ‘thermal’ regime leads to similar propagation loss as the ‘athermal’ regime.

The measured numerical aperture of these waveguides was  $\sim 0.06$ , and the change in refractive index ( $\Delta n = n_{\text{core}} - n_{\text{cladding}}$ ) was estimated to be  $(9 \pm 0.5) \times 10^{-4}$  with an estimated ‘general’ positive refractive index contrast of  $\sim 5.3 \times 10^{-4}$  ( $\Delta = (n_{\text{core}}^2 - n_{\text{cladding}}^2) / 2n_{\text{core}}^2$ ). We are considering techniques to reduce the ellipticity of the waveguides such as using slit beam shaping [17,18] to make the waveguides relatively circular, and also considering writing modifications close to each other to realize a stress guiding waveguide. Annealing the waveguides at a temperature lower than the glass transition temperature may also help in reducing built-in stress, potentially contributing to a reduction of loss from these tear-drop structures.

Figure 5 shows the experimental setup used for operation of the waveguide laser. A single-mode, fiber-coupled  $P = 900$  mW diode operating at 976 nm was used to pump the waveguide (in-line optical isolator used). The 1.5 mm diameter collimated pump light was focused using a  $f = 30$  mm lens to achieve a beam of  $\sim 22 \mu\text{m}$  spot size with the NA nearly matching the observed NA of the waveguide. A butt-coupled laser cavity composed of a  $R = 90\%$  OC with  $L = 13$  mm long waveguides was investigated. This pump focusing condition produced  $\sim 15$  mW of laser output. Laser performance is shown in Fig. 6(a) which represents the output power produced by varying the incident pump power. A linear fit to the data indicated a laser slope efficiency of  $\sim 5\%$ . We attribute the ‘noisy’ slope efficiency to etalons formed between the mirrors and high refractive index glass. Inset to Fig. 6(a) is a near-field image of the single-lobed laser mode, with the  $M^2$  measured to be  $\sim 3$ , indicating that this is not a single transverse mode laser cavity. This is likely attributed to both the non-symmetrical waveguide cross-section and the non-uniform refractive index profile of the waveguide.



**Fig. 5.** Laser setup to pump the  $\sim 24 \mu\text{m}$  diameter waveguide with a  $f = 30$  mm focusing lens producing a  $\sim 22 \mu\text{m}$  spot size. High transmission IC and  $R \sim 90\%$  OC were butt-coupled to the chip containing waveguides. The output was filtered using a short-pass filter to remove the pump and was observed using an infrared camera (Ophir SP503U) and a power meter.

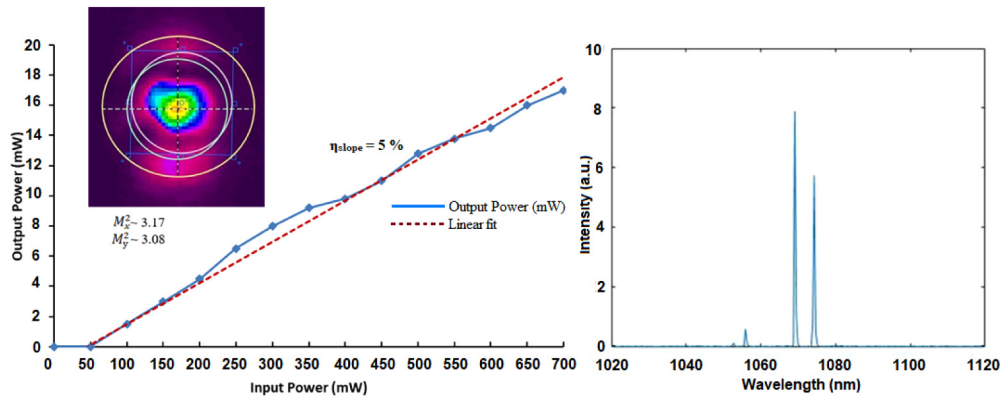


**Fig. 6.** (a): Output power as a function of incident pump power for the waveguide laser giving an incident slope efficiency of  $\sim 5\%$ . The near-field image of the waveguide laser mode is also presented in the inset. (b) Wavelength of the free running  $\text{Yb}^{3+}$  doped germanate GPGN L  $\sim 13$  mm waveguide laser showing emission from 1055 nm to 1075 nm.

Figure 6(b) shows the broad spectral emission of the free-running waveguide laser peaking around 1069 nm and 1075 nm. A small laser peak was also observed at 1055 nm showing the broad gain of the spectrally free-running laser. A wavelength shift is observed in the microchip and waveguide lasers, which is dependent on the length of the laser cavity. For the microchip laser, the cavity length is 4.5 mm while the waveguides are 13 mm long and are thus responsible for the red shift of wavelength from 1052 nm in the microchip laser to 1075 nm in the longer waveguide laser.

#### 4. Conclusion

We report the first  $\text{Yb}^{3+}$ -doped germanate ‘microchip’ laser, and ultra-fast laser written waveguide laser. Both lasers are based on the same 3.6 wt%  $\text{Yb}^{3+}$  doped lead-germanate GPGN sample, and are configured for semi-monolithic operation with resonator mirrors butted to the ends of the gain chip. For the  $L = 4.5$  mm microchip laser, we achieved 51 mW maximum average output power (peak power of 0.51 W) for 700 mW average pump power at 976 nm with a slope efficiency of  $\sim 30\%$  and lasing threshold of  $\sim 100$  mW (average power). We also investigated the effect of beam spot-size on the output power and the slope efficiency of the microchip laser. For the  $L = 13$  mm waveguide laser, we achieved  $\sim 15$  mW maximum output power for 700 mW average pump power at 976 nm. The broad spectral laser output was observed to emit discrete lines at 1069 nm and 1075 nm. We are further investigating the effects of different parameters on the shape of waveguides and working to optimize the laser performance.

#### Funding

AOARD (FA2386-16-1-4068); ARC LIEF grant (LE140100042).

#### Acknowledgements

The authors acknowledge J.E. Moffatt for helping in taking fluorescence measurements. The authors would like to acknowledge the OptoFab node of the Australian National Fabrication Facility supported by the Commonwealth and South Australian State Government. M. Khalid acknowledges the University of South Australia for a University President Scholarship.



## References

1. J. Siegel, J. M. Fernández-Navarro, A. Garcia-Navarro, V. Diez-Blanco, O. Sanz, J. Solis, F. Vega, and J. Armengol, "Waveguide structures in heavy metal oxide glass written with femtosecond laser pulses above the critical self-focusing threshold," *Appl. Phys. Lett.* **86**(12), 121109 (2005).
2. C. B. De Araujo, D. S. da Silva, T. A. Alves de Assumpção, L. R. P. Kassab, and D. M. da Silva, "Enhanced optical properties of germanate and tellurite glasses containing metal or semiconductor nanoparticles," *Sci. World J.* **2013**, 1–13 (2013).
3. H. T. Munasinghe, A. Winterstein-Beckmann, C. Schiele, D. Manzani, L. Wondraczek, S. Afshar, T. M. Monro, and H. Ebendorff-Heidepriem, "Lead-germanate glasses and fibers: a practical alternative to tellurite for nonlinear fiber applications," *Opt. Mater. Express* **3**(9), 1488–1503 (2013).
4. X. Jiang, J. Lousteau, B. Richards, and A. Jha, "Investigation on germanium oxide-based glasses for infrared optical fibre development," *Opt. Mater.* **31**(11), 1701–1706 (2009).
5. V. Kamynin, A. Kurkov, and V. Mashinsky, "Supercontinuum generation up to 2.7  $\mu\text{m}$  in the germanate-glass-core and silica-glass-cladding fiber," *Laser Phys. Lett.* **9**(3), 219–222 (2012).
6. R. Xu, J. Pan, L. Hu, and J. Zhang, "2.0  $\mu\text{m}$  emission properties and energy transfer processes of Yb 3+/Ho 3+ codoped germanate glass," *J. Appl. Phys.* **108**(4), 043522 (2010).
7. X. Fan, P. Kuan, K. Li, L. Zhang, D. Li, and L. Hu, "Spectroscopic properties and quenching mechanism of 2  $\mu\text{m}$  emission in Ho 3+ doped germanate glasses and fibers," *Opt. Mater. Express* **5**(6), 1356–1365 (2015).
8. P.-W. Kuan, X. Fan, X. Li, D. Li, K. Li, L. Zhang, C. Yu, and L. Hu, "High-power 2.04  $\mu\text{m}$  laser in an ultra-compact Ho-doped lead germanate fiber," *Opt. Lett.* **41**(13), 2899–2902 (2016).
9. J. Wu, Z. Yao, J. Zong, and S. Jiang, "Highly efficient high-power thulium-doped germanate glass fiber laser," *Opt. Lett.* **32**(6), 638–640 (2007).
10. D. Choudhury, J. R. Macdonald, and A. K. Kar, "Ultrafast laser inscription: perspectives on future integrated applications," *Laser Photonics Rev.* **8**(6), 827–846 (2014).
11. D. S. da Silva, N. U. Wetter, W. de Rossi, R. E. Samad, and L. R. Kassab, "Femtosecond laser-written double line waveguides in germanate and tellurite glasses," in *Laser Applications in Microelectronic and Optoelectronic Manufacturing (LAMOM) XXIII* (International Society for Optics and Photonics 2018), p. 105191B.
12. F. Fusari, R. Thomson, G. Jose, F. Bain, A. Lagatsky, N. Psaila, A. Kar, A. Jha, W. Sibbett, and C. Brown, "Lasing action at around 1.9  $\mu\text{m}$  from an ultrafast laser inscribed Tm-doped glass waveguide," *Opt. Lett.* **36**(9), 1566–1568 (2011).
13. D. M. Da Silva, L. R. P. Kassab, M. Olivero, T. B. Lemos, D. V. Da Silva, and A. Gomes, "Er<sup>3+</sup> doped waveguide amplifiers written with femtosecond laser in germanate glasses," *Opt. Mater.* **33**(12), 1902–1906 (2011).
14. V. Denisov, S. Tin'kova, L. Denisova, and L. Irtyugo, "Thermal conductivity of the PbGeO<sub>3</sub> and PbGe<sub>3</sub>O<sub>7</sub> glasses," *Phys. Solid State* **53**(10), 2025–2027 (2011).
15. L. A. Irtyugo, L. T. Denisova, V. M. Denisov, N. V. Belousova, and A. S. Samoilo, "Thermal Expansion of Lead Germanate Glass," *J. Sib. Fed. Univ., Chem.* **1**, 37–40 (2012).
16. S. Gross, M. Ams, G. Palmer, C. T. Miese, R. J. Williams, G. D. Marshall, A. Fuerbach, D. G. Lancaster, H. Ebendorff-Heidepriem, and M. J. Withford, "Ultrafast laser inscription in soft glasses: a comparative study of athermal and thermal processing regimes for guided wave optics," *Int. J. Appl. Glass Sci.* **3**(4), 332–348 (2012).
17. M. Ams, G. Marshall, D. Spence, and M. Withford, "Slit beam shaping method for femtosecond laser direct-write fabrication of symmetric waveguides in bulk glasses," *Opt. Express* **13**(15), 5676–5681 (2005).
18. P. Salter, A. Jesacher, J. Spring, B. Metcalf, N. Thomas-Peter, R. D. Simmonds, N. Langford, I. Walmsley, and M. J. Booth, "Adaptive slit beam shaping for direct laser written waveguides," *Opt. Lett.* **37**(4), 470–472 (2012).